DETECTION OF HIGH ORDER M-ARY QAM SYMBOLS UNDER TRANSMITTER NONLINEARITIES

A THESIS SUBMITTED TO
THE GRADUATE SCHOOL OF NATURAL AND APPLIED SCIENCES
OF
MIDDLE EAST TECHNICAL UNIVERSITY

BY

ZİYA GÜLGÜN

IN PARTIAL FULFILLMENT OF THE REQUIREMENTS
FOR
THE DEGREE OF MASTER OF SCIENCE
IN
ELECTRICAL AND ELECTRONICS ENGINEERING

JULY 2018

Approval of the thesis:

DETECTION OF HIGH ORDER M-ARY QAM SYMBOLS UNDER TRANSMITTER NONLINEARITIES

submitted by **ZİYA GÜLGÜN** in partial fulfillment of the requirements for the degree of **Master of Science in Electrical and Electronics Engineering Department, Middle East Technical University** by,

Prof. Dr. Halil Kalıpçılar
Dean, Graduate School of **Natural and Applied Sciences** ______________

Prof. Dr. Tolga Çiloğlu
Head of Department, **Electrical and Electronics Engineering** ______________

Prof. Dr. Ali Özgür Yılmaz
Supervisor, **Electrical and Electronics Engineering Dept., METU** ______________

Examining Committee Members:

Prof. Dr. Yalçın Tanık
Electrical and Electronics Engineering Dept., METU ______________

Prof. Dr. Ali Özgür Yılmaz
Electrical and Electronics Engineering Dept., METU ______________

Prof. Dr. Engin Tuncer
Electrical and Electronics Engineering Dept., METU ______________

Assoc. Prof. Dr. Cenk Toker
Electrical and Electronics Engineering Dept., Hacettepe University ______________

Assist. Prof. Dr. Gökhan Güvensen
Electrical and Electronics Engineering Dept.,METU ______________

Date: ______________

I hereby declare that all information in this document has been obtained and presented in accordance with academic rules and ethical conduct. I also declare that, as required by these rules and conduct, I have fully cited and referenced all material and results that are not original to this work.

Name, Last Name: ZİYA GÜLGÜN

Signature :

ABSTRACT

DETECTION OF HIGH ORDER M-ARY QAM SYMBOLS UNDER TRANSMITTER NONLINEARITIES

GÜLGÜN, ZİYA
M.S., Department of Electrical and Electronics Engineering
Supervisor : Prof. Dr. Ali Özgür Yılmaz

July 2018, 41 pages

We will investigate the nonlinear effects of power amplifiers on large constellation Quadrature Amplitude Modulation (QAM) in this study. A more than potential feat to enhance transmission rates in next generation wireless networks is high order QAM along with mm-wave transmission. Meanwhile, different types of nonlinearities in the transmitter side may hamper the transmitter rate and decrease receiver performances. From literature, outermost constellation points of QAM schemes are usually more adversely affected by these deteriorations. To observe these effects, the Rapp and Saleh models that consider only amplitude deformation and amplitude in conjunction with phase deformation respectively are utilized. Error vector magnitude (EVM) of each QAM symbol is evaluated to discriminate error variances of each symbol. It is observed that in-phase and quadrature errors originating from the Rapp model can be assumed as independent. On the contrary, power amplifier with the Saleh model creates error such that in-phase and quadrature parts of the errors are not independent. According to our observations, the variances of in-phase and quadrature errors may not even be equal to each other. By accounting for all above issues, receivers that con-

sider unequal EVM distribution for both models are proposed and their performances are compared with those of other receivers that exert average EVM for decoding. In addition to these receivers, a practical receiver is proposed that works on quantized observations based on a look-up table that keeps log-likelihood ratios to reduce computational complexity. Furthermore in this work, mismatched achievable rates of the equivalent nonlinear channels are presented to evaluate decoding thresholds of the receivers.

Keywords: Nonlinear Characteristic of Power Amplifiers, Mismatched Decoding, Nonlinear Channels, High Order QAM, Warped QAM, Nonlinear ISI, EVM

ÖZ

GÖNDERİCİ BOZUKLUĞU ALTINDAKİ YÜKSEK DERECELİ M-LİK QAM SEMBOLLERİNİN TESPİTİ

GÜLGÜN, ZİYA
Yüksek Lisans, Elektrik ve Elektronik Mühendisliği Bölümü
Tez Yöneticisi : Prof. Dr. Ali Özgür Yılmaz

Temmuz 2018 , 41 sayfa

Bu çalışmada, güç yükselteclerin doğrusal olmayan etkilerinin gelecek nesil kablosuz haberleşme adaylarından biri olan yüksek dereceli QAM üzerine etkileri incelenmiştir. Verici tarafındaki çeşitli doğrusal olmayan bozucu etkiler alıcı tarafının performansının düşmesine sebep olmaktadır. Literatürdeki gözlemlerimize göre, QAM yıldız kümesinin dışındaki noktalar bu etkilerden genellikle daha fazla etkilenmektedir. Bu etkiyi gözlemlemek için sadece genlik bozulmasını inceleyen Rapp modeli ve genlikle beraber faz bozulmasını inceleyen Saleh modelinden yararlanılmıştır. Her QAM sembolünün EVM değeri incelenmiştir. Gözlemlere göre Rapp modelinden kaynaklı eş fazlı ve dördün kısmındaki bozulmalar bağımsız olarak sayılabilir. Fakat Saleh modelinin oluşturduğu bozulmalar gözlemlerimize göre bağımsız değildir. Gene gözlemlerimize göre bozulmaların büyüklüğü birbirine eşit bile olmayabilir. Yukarıda anlatılanların hepsini dikkate alarak, yıldız kümesi üzerindeki tekdüze olmayan EVM dağılımını göz önünde bulunduran alıcılar her iki model için de önerilmiştir ve bu alıcıların performansı ortalama EVM değerini değerlendiren klasik alıcılarla karşılaştırılmıştır. Ayrıca, işlem karmaşıklığını azaltmak için alıcı tarafında gözlemlenen sembolleri niceleyen alıcı yapısı önerilmiştir. Alıcı, nicemlenmiş sembollere arama tablosundan olasılık oranı vermekte ve buna göre çözümleme yapmaktadır. Ayrıca, bu çalışmada alıcların çözümleme eşik değerlerini kıyaslamak için doğrsual olmayan kanallar için uyumsuz başarım hızları ifade edilmiştir.

Anahtar Kelimeler: Güç Yükselteclerin Doğrusal Olmayan Karaketeristikleri, Uyumsuz Çözümleme, Doğrusal Olmayan Kanallar, Yüksek Dereceli QAM, Bükülmüş QAM, Doğrusal Olmayan ISI, EVM

To my uncle

ACKNOWLEDGMENTS

First and foremost, I would like to express my greatest gratitude to my supervisor, Prof. Dr. Ali Özgür Yılmaz for providing me with guidance and advice on research problems. Without his illuminating comments on my work, I could not have finished my thesis. Apart from this, he showed me how a researcher should evaluate a problem and proceed through it. This is valuable for me as a researcher who has just begun the academic life.

In addition to my supervisor, I would like thank Dr. Gökhan Güvensen for his special comments and contributions to my works. It was a pleasure to talk with him about not only communication theory but also almost everything.

I would also like to thank and appreciate invaluable friendship and support of Ali Bulut Üçüncü during my master time. I extremely enjoyed fruitful discussion about technical topics. Furthermore, I would like to thank him for the pleasant and enjoyable talks.

I also want to acknowledge the financial support that the scientific and technological research council of Turkey (TÜBİTAK) granted me during my master period.

I am very grateful to my aunt, Elmas Gülgün, and my deceased uncle, Şükrü Gülgün, who do not have children and they placed me and my brother in their heart as if we were their children. I would like to emphasize that my uncle graduated from METU civil engineering led me to become an engineer and be interested in mathematics.

I would also like to give special thanks to my girl friend Çınar Delibal. She has gave me her endless support, love and motivation for seven years. I admire her optimistic personality. She has always encouraged me when I have went to the wall.

Last but not least, I would like to express my deepest gratitude to my parents, Ayşe and Devrim Gülgün (deceased) with all my heart. I genuinely owe all my achievements to them. I also thank them to give a brother, Mert Gülgün who supports and encourges me for hardships of the life.

TABLE OF CONTENTS

LIST OF TABLES

TABLES

LIST OF FIGURES

FIGURES

LIST OF ABBREVIATIONS

BER	Bit error rate
BICM	Bit interleaved Coded Modulation
DPD	Digital Predistortion
ECC	Error Correction Codes
EVM	Error Vector Magnitude
IBO	Input Backoff
ISI	Inter-symbol Interference
LDPC	Low Density Parity Check
LLR	Log Likelihood Ratio
PDF	Probability Density Function
OBO	Output Backoff
QAM	Quadrature Amplitude Modulation
SNR	Signal to Noise Ratio

CHAPTER 1

INTRODUCTION

High order quadrature amplitude modulation (QAM) schemes such as 1024QAM, 4096QAM that lead to high spectral efficiency are considered for next generation wireless networks to facilitate mobile data growth [1], [2]. However, transmitted signal can be distorted heavily with large constellation QAM by the nonidealities such as local oscillator leakage, nonlinear characteristics of power amplifier etc. and these distortions may decrease receiver performance significantly.

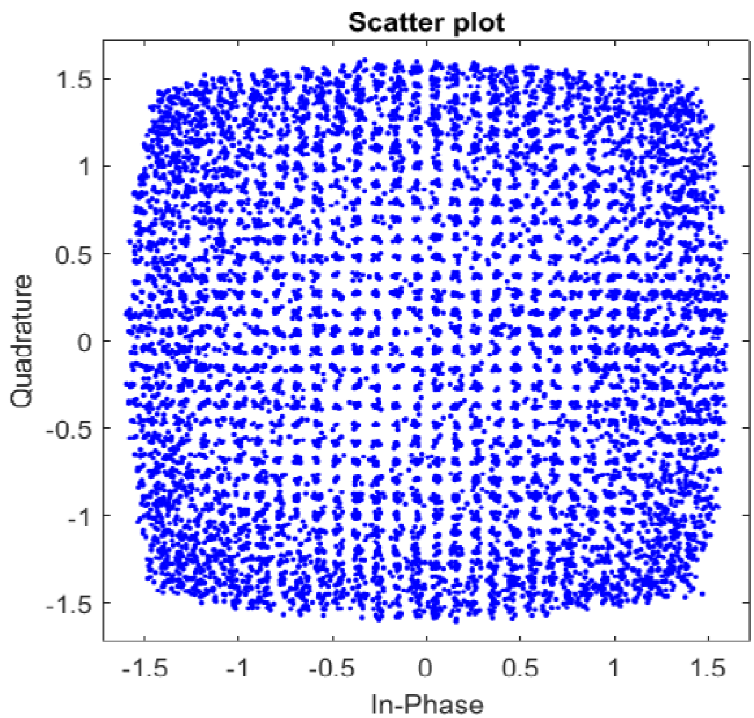

Figure 1.1: 1024 QAM constellation points passed through a power amplifier with the Rapp model

In particular, larger constellations are more adversely affected by these nonlinearities. Outermost constellation points that have relatively more power are usually more distorted and this imperfection degrades the overall receiver performance. Figure 1.1 and Figure 1.2 are examples of received symbol constellations corresponding to 1024 QAM passed through power amplifiers that run with the Rapp and Saleh models respectively. These figures are obtained without thermal noise. The reason for the clouds around the symbols is only nonlinearity of the power amplifiers. From the figures, the outermost constellation points are more distorted by the power amplifier models since the clouds around the outermost constellation points are larger than the other clouds.

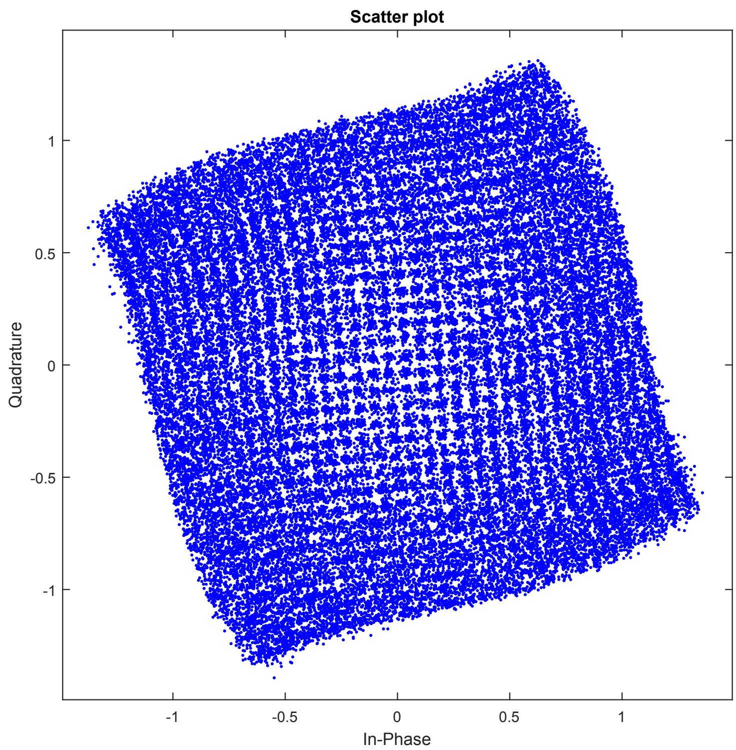

Figure 1.2: 1024 QAM constellation points passed through a power amplifier with the Saleh model

In [3], 16QAM and the Saleh model were utilized in the transmitter and the distortion was modelled with zero mean circularly symmetric Gaussian distribution in order to use turbo equalization on the receiver side. For the high order QAM this is not a suitable model. From Figure 1.2, the variances of in-phase and quadrature errors may not be equal to each other and the correlation between in-phase and quadrature errors may exist. Furthermore, the error magnitudes vary from symbol to symbol depending on symbol's power, i.e., symbol's place on the constellation as it can be seen from Figure 1.1 and 1.2 and [3] does not consider it.

In order to linearize the structure, digital predistortion (DPD) can be performed in the transmitter side before the power amplifier [4]. Basically, the transmitted signal is modified by DPD based on nonlinearity characteristics. However, perfect linearization is not possible and as observed in various studies the nonlinearities still remain in the transmitted signal. For example, [5] and [6] attain significant enhancements for linearization, but perfect linearization cannot be reached. Due to this imperfect linearization, this heterogeneous variation of error across the clouds as in Figure 1.1 and Figure 1.2 remains even though DPD is utilized and is referred as nonuniform error vector magnitude (EVM) in [7].

In this thesis, achievable rates of the nonlinear channels that stem from power amplifier models are evaluated. These achievable rate expressions will be explained in next chapters. Furthermore, the receivers that take the error variance of each symbol into account for both power amplifier models are proposed. The performances of the proposed receivers and those of conventional receivers that work with average error variance of the received symbols are compared. Toward practical implementation, a receiver that quantizes observations and decodes according to a look-up table that contains log-likelihood ratios is proposed to reduce the computational complexity.

The contributions of this thesis can be summarized as:

- Achievable rates of nonlinear channels that create nonuniform EVM on the constellation are evaluated.
- Performances of receivers that consider nonuniform EVM are compared with those of conventional receivers that work with average EVM of the constellations.
- Performance of a receiver that quantizes observations and operate according to a look-up table is evaluated.

CHAPTER 2

SYSTEM MODEL

In this chapter transmitter and receiver side of the system model are to be explained. We consider a simplified model in which only the nonlinearity effect of the power amplifier is accounted for. Although there may be nonlinear effects originating from various stages such as mixers, local oscillators and power amplifier drivers, we combine all their effects into the power amplifier as an abstraction and refer to the problem as the power amplifier nonlinearity since it is usually the dominant factor. Receiver thermal noise is also discarded so as to focus only on the rate limitations due to transmit nonlinearities. In addition to these system impairments, antenna of the transmitter and that of the receiver are so close that path loss, fading, Doppler effect etc. do not exist in the model.

2.1 Transmitter Side

One can examine the schematic of the transmitter side in Figure 2.1.

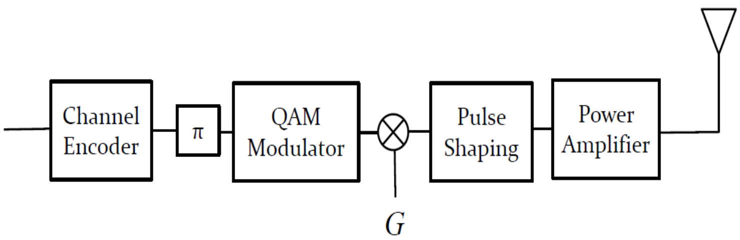

Figure 2.1: Transmitter Side

Each block will be explained one by one.

2.1.1 Channel Encoder

The first block is channel encoder in the transmitter side. In this work, Low Density Parity Check (LDPC) codes whose performance limit and Shannon limit are close to each other were used [8].

2.1.2 Interleaver

Interleaver block is replaced after the channel encoder block. Interleaver takes the bit sequence produced by the encoder and gives an output bit sequence in a different order. Albeit error correction codes (ECC) diminish the errors, interleaver makes robust the communication system for burst error. The cost for using interleaver is that bit interleaved coded modulation (BICM) capacity cames close but does not always achieve the coded modulation capacity as stated in [9].

2.1.3 QAM Modulator

The modulation type is Quadrature Amplitude Modulation (QAM). In this thesis, 1024 QAM was used. The symbols were produced with unit average power, i.e., $E[|X|^2] = 1$, where X is a random generated symbol from a fixed alphabet.

2.1.4 Gain Block

After the QAM modulator, there is a gain block which adjusts the transmit power. When the gain G is small, we operate in the linear region of the power amplifier and error vector magnitude (EVM) is small, albeit the transmit power is low. Hence we make use of the parameter G to determine the power backoff level and vary EVM.

2.1.5 Pulse Shaping

In the pulse shaping part we used a root raised cosine filter having unit energy with 0.25 roll-off factor, 5 samples per symbol and 201 taps in total. This choice of parameters ensures an operation close to an analog model which is necessary for observing the effects of power amplifier. Figure 2.2 illustrates the filter with given parameters.

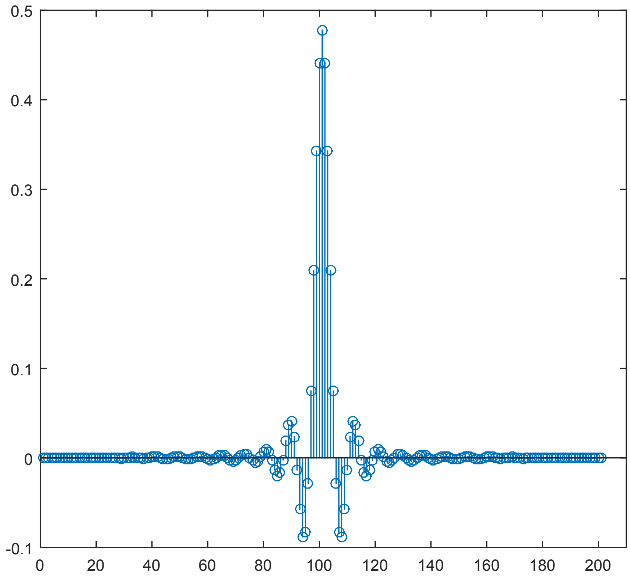

Figure 2.2: Root Raised Cosine Filter with 0.25 roll of factor, 5 samples per symbol and 201 taps

2.1.6 Power Amplifier

In the literature, there are many power amplifier models that can be categorized as either memoryless power amplifier or power amplifier considering memory. In this work, two common memoryless power amplifier models, Saleh and Rapp models, were utilized.

2.1.6.1 Rapp Model

Rapp model is a class of AM-AM amplifier models. Namely, the Rapp model creates only amplitude distortion and the input-output characteristic can be expressed as [10]:

$$S_{in}(t) = A_{in}(t) \cdot e^{j\phi_{in}(t)}, \tag{2.1}$$

$$S_{out}(t) = \frac{v \cdot A_{in}(t)}{(1 + (v \cdot A_{in}(t)/A_0)^{2p})^{\frac{1}{2p}}} \cdot e^{j\phi_{in}(t)} \tag{2.2}$$

where $S_{in}(t)$ is the input signal, $A_{in}(t)$ and $\phi_{in}(t)$ are the amplitude and the phase of the input signal respectively, $S_{out}(t)$ is the output signal. The parameters v and A_0 set the saturation level of the model and p determines the nonlinearity characteristic relative to the input signal power. As obvious from (2.1) and (2.2), the Rapp model generates only amplitude distortion. In this work, v and A_0 are taken as one and one Volt to normalize the saturation level and p is set equal to two according to [11]. Nonlinear characteristic of the Rapp model can be seen from Figure 2.3 for the given

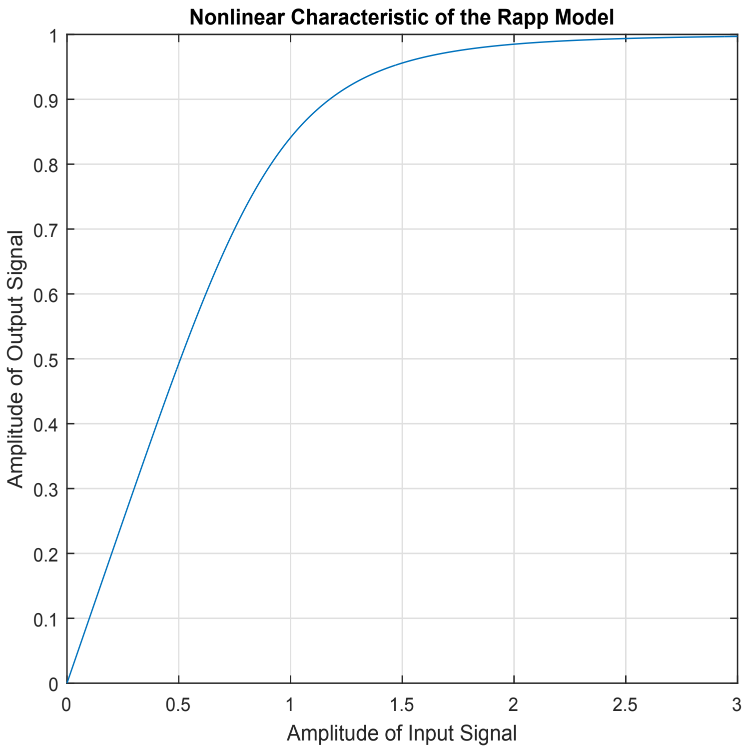

Figure 2.3: Nonlinear Characteristic of the Rapp model with parameters $p = 2, A_0 = 1, v = 1$

parameters.

2.1.6.2 Saleh Model

Saleh model is an another common power amplifier model which considers not only AM-AM distortion but also AM-PM distortion. For this model, the input-output relation characteristic can be modelled as [12]:

$$S_{in}(t) = A_{in}(t) \cdot e^{j\phi_{in}(t)}, S_{out}(t) = G(t) \cdot e^{j\phi_{in}(t)} \cdot e^{j\Phi(t)}, \tag{2.3}$$

$$G(t) = \frac{g_0 \cdot A_{in}(t)}{1 + (A_{in}(t)/A_0)^2}, \Phi(t) = \frac{\alpha \cdot A_{in}^2(t)}{1 + \beta \cdot A_{in}^2(t)}, \tag{2.4}$$

where $S_{in}(t)$ is the input signal, $A_{in}(t)$ and $\phi_{in}(t)$ are the amplitude and the phase of the input signal respectively, $S_{out}(t)$ is the output signal. $G(t)$ is magnitude of $S_{out}(t)$ and $\Phi(t)$ represents the phase distortion in radian. The parameters g_0 and A_0 determine the amplitude distortion and are taken as 1 and 2 for this work that are standart values [13]. The parameters α and β determine the phase distortion and are taken as $\pi/4$ and 0.25 for this work. By setting these parameters into (2.3) and (2.4), nonlinear characteristics of the power amplifier model are observed as in Figure 2.4. As deduced from Figure 2.4, signals having more power are affected more by nonlinear characteristics of the power amplifier.

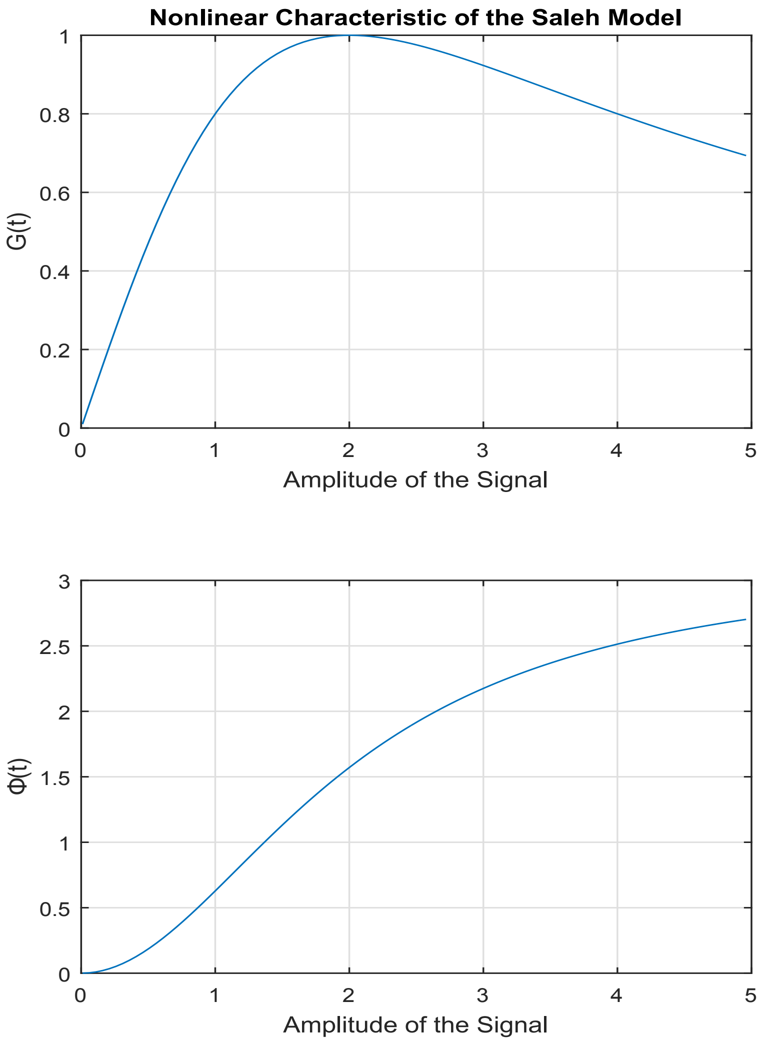

Figure 2.4: Nonlinear Characteristic of the Saleh model with parameters $g_0 = 1, A_0 = 2, \alpha = \pi/4, \beta = 0.25$

2.1.7 Power Amplifier Parameters

Power amplifier parameters are crucial especially for designing the input signal. Let us define a parameter P_{out}^{sat} which is the maximum output power given by a power amplifier and define P_{in}^{sat} which is the minimum output power required to obtain P_{out}^{sat}. After defining these parameters, input backoff (IBO) and output backoff (OBO) can be written as [14]:

$$IBO = \frac{P_{in}^{sat}}{P_{in}}, \tag{2.5}$$

$$OBO = \frac{P_{out}^{sat}}{P_{out}} \tag{2.6}$$

where P_{in} and P_{out} are input signal power and output signal power. From 2.5 and 2.6, these parameters can be seen as a tradeoff between nonlinear distortion and signal power. Namely, if IBO or OBO increases, power of a signal and distortion will decrease and vice a versa.

2.2 Receiver Side

In this section, the receiver side of the model is going to be explained. One can examine the schematic of the system model's receiver side in Figure 2.5. The matched filter is the time reverse of the pulse shape filter. Since the pulse shape filter that was used in this work is real and even symmetric, the matched filter is the same pulse shape filter as in Figure 2.2. After the matched filter block, the demodulator block which calculates log likelihood ratio (LLR) values can be seen. In this work, 1024 QAM demodulator block was used. After the matched filter, deinterleaver is followed by a LDPC Decoder.

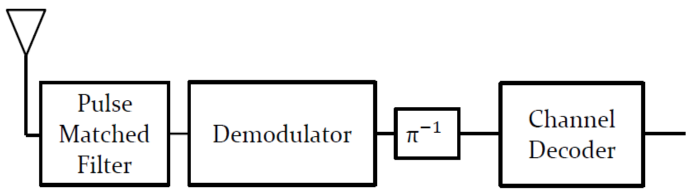

Figure 2.5: Receiver Side

CHAPTER 3

NONLINEAR CHANNEL MODELS

In this thesis, the error originating from the nonlinearity of the power amplifiers is modelled as an additive white Gaussian noise the same as thermal noise. Indeed, if the receiver knows the nonlinear characteristic exactly, a maximum likelihood sequence detector will operate perfectly. In other words, it produces no bit error in the absence of other destructive effects since the system model is deterministic. Such a detector is currently above practical reach. Therefore, the effects of neighboring symbols on a particular symbols are regarded as random noise instead of computing the error terms due to these effects. Based on this approach, we develop channel models.

The nonlinear channels have negative effects on signals in time domain such as warping and nonlinear inter-symbol interference (ISI) and in frequency domain such as out-of-band radiation [15]. In this work, we mainly focus on warping and nonlinear ISI effects to be further explained in this chapter.

3.1 Warping and Nonlinear ISI

Warping and nonlinear ISI are mainly responsible for the distortion. Figure 1.1 is an example of received symbols' constellation corresponding to 1024 QAM passed through a power amplifier with the Rapp model. Due to saturated power of the amplifier, corner constellation points, i.e., constellation points having more power relatively, are closer to each other than the inner constellation points. This kind of constellation is referred to as a warped constellation [16].

Nonlinear ISI can occur since the matched filter may not be matched with the transmitted pulse shape after passing through a nonlinear device. In order to clarify this point, consider the scenario with a power amplifier of linear gain g :

$$y(t) = g \sum_n x_n h(t - nT), \tag{3.1}$$

which is expressed in terms of the transmitted signal with symbols x_n and root raised cosine pulse $h(t)$. The output of the matched filter can be written as

$$r(t) = y(t) * h(-t) = g \sum_n x_n \widetilde{h}(t - nT), \tag{3.2}$$

where $\widetilde{h}(t)$ is a Nyquist pulse and ISI will not exist if the signal is sampled with sampling period T and ideal synchronization [17]. Let us analyze the same scenario with a nonlinear power amplifier. The power amplifier characteristic, say function f, can be any function that has nonlinearity. Owing to nonlinearity, (3.1) and (3.2) become

$$y(t) = f\left(\sum_n x_n h(t - nT)\right), \tag{3.3}$$

$$r(t) = y(t) * h(-t) = f\left(\sum_n x_n h(t - nT)\right) * h(-t). \tag{3.4}$$

It can be observed from (3.4) that the presence of Nyquist pulse shaping and ideal sampling cannot eliminate ISI perfectly due to transmit nonlinearities. This ISI can be modelled with Volterra series that are general nonlinear polynomial expansions [18]. For discrete time, the Volterra equation can be written as [18]

$$y_n = \sum_i g_i x_{n-i} + \sum_i \sum_j \sum_k g_{i,j,k} x_{n-i} x_{n-j} x^*_{n-k} + \dots \tag{3.5}$$

where y_n is the output at time n, x_n is the input at time n, g_i is a coefficient of linear tap x_{n-i} and $g_{i,j,k}$ is a coefficient of third order tap $x_{n-i} x_{n-j} x^*_{n-k}$. To clarify ISI terms, (3.5) can be rewritten as

$$y_n = \underbrace{g_0 x_n}_{\text{transmitted symbol}} + \underbrace{\sum_{i \neq 0} g_i x_{n-i} + \sum_i \sum_j \sum_k g_{i,j,k} x_{n-i} x_{n-j} x^*_{n-k} + \dots}_{\text{ISI}} \tag{3.6}$$

Nonlinear equalizers, either adaptive [19] or non-adaptive [20], [21] are proposed in the receiver side to handle nonlinear ISI in (3.6). In this work, nonlinear ISI is considered as an additive noise with a mismatched distribution function by the receivers which will be explained in later parts.

3.2 Nonlinear Channel Model for the Rapp Model

We employed a simple model for the relation between the transmitted and received symbols that is dominantly utilized in literature [22], [23], [24], albeit many other models can be proposed. The warping is modelled with a single scalar and all the remaining effects are incorporated into a noise term as in

$$\mathbf{y} = \alpha \mathbf{x} + \mathbf{w}, \tag{3.7}$$

where $\mathbf{x}$ is the vector of transmitted M-QAM symbols, $\mathbf{y}$ is the vector of sampled observations, $\mathbf{w}$ is the error vector and α is the warping coefficient. For the model given in (3.7), EVM can be calculated for N dimensional $\mathbf{x}$ and $\mathbf{y}$ vectors as [25]

$$EVM = \sqrt{\frac{\sum_{k=1}^{N} |y_k - \alpha x_k|^2}{\sum_{k=1}^{N} |\alpha x_k|^2}}, \tag{3.8}$$

where the numerator reflects error variance and the denominator perform normalization. The least squares solution of (3.7) gives the parameter α such that

$$\alpha = \frac{\mathbf{y}^H \mathbf{x}}{||\mathbf{x}||^2}. \tag{3.9}$$

The parameter α will be a real scalar if the model operates in the linear region of a power amplifier since the Rapp model considers only amplitude distortion and phase of the input signal and that of the received signal are equal to each other. On the contrary, if the model operates in the nonlinear region, the parameter α will become a complex scalar due to nonlinear ISI.

(3.7), (3.8) and (3.9) can be used for finding the average EVM of the model. However, since EVM varies from symbol to symbol, EVM of each constellation point must be evaluated separately. To do that, one cannot simply transmit a vector consisting only of the symbol a_i in which i changes from 1 to M for M-ary QAM scheme since this would mask the ISI which is randomly formed by the randomly generated neighboring symbols and the transmit nonlinearities. For this purpose, very long vectors of $\mathbf{x}$ and $\mathbf{y}$ are first generated and a subvector of $\mathbf{y}$, that is $\mathbf{y}_i$, is arranged for indices with symbol a_i being the transmitted symbol. To clarify this point, suppose $\mathbf{x}$ is produced randomly with $\mathbf{x} = (\begin{bmatrix} a_{20} & a_{14} & a_M & a_i & \dots & a_i & a_{150} \end{bmatrix}_{1\times N})^T$. In the receiver side, the observation samples corresponding to a_i can be written as a vector form such that

$\mathbf{y_i} = (\begin{bmatrix} y_{i_1} & y_{i_2} & y_{i_3} & y_{i_4} & \dots & y_{i_{K_i}} \end{bmatrix}_{1\times K_i})^T$, with K_i being the number of a_i in $\mathbf{x}$. Obviously, the members of $\mathbf{y_i}$ are not equal to each other. After this clarification, the relation between a_i and $\mathbf{y}_i$ can be written as

$$\mathbf{y}_i = \alpha_{x_i}\mathbf{x}_i + \mathbf{w}_i, \tag{3.10}$$

where $\mathbf{x}_i$ is the vector which consists of only a_i and $\mathbf{w}_i$ is the error vector corresponding to a_i. The least squares solution for α_i can be expressed as

$$\alpha_i = \frac{\mathbf{y}_i^H \mathbf{x}_i}{||\mathbf{x}_i||^2}. \tag{3.11}$$

The least squares solution minimizes the norm of $\mathbf{w}_i$ and guarantees that $\mathbf{x}_i$ and $\mathbf{w}_i$ are orthogonal. The variance can be found by

$$\sigma_i^2 = \frac{\sum_{n=1}^{K_i} |y_{i,n} - \alpha_i x_{i,n}|^2}{K_i}, \tag{3.12}$$

where $y_{i,n}$ and $x_{i,n}$ are the n^{th} elements of the vectors $\mathbf{y}_i$ and $\mathbf{x}_i$ respectively and σ_i^2 is a measure of error magnitude, that is the variance of error around symbol a_i. For M-QAM transmission, we have M distinct α_i and σ_i^2 values that can be used on the receiver side.

3.3 Nonlinear Channel Model for the Saleh Model

The channel for the Saleh model is slightly different than the channel for the Rapp model with three main reasons. The first reason is that the received symbols which can be seen in Figure 1.2 are rotated when the Saleh model is used for the power amplifier. The second reason is that the variances of in-phase distortion and quadrature distortion may not be equal to each other. In addition to this, distortions of in-phase and quadrature parts may be correlated especially for the outermost constellation points.

To express the rotation in Figure 1.2, one can utilize (3.10) with a complex α_{x_i}. In other words, to express the rotation it requires two unknown values that correspond to magnitude and phase of complex α_{x_i}. A 2×2 matrix can also yield the rotation and this matrix is called the rotation matrix [26]. One can see the rotation of the

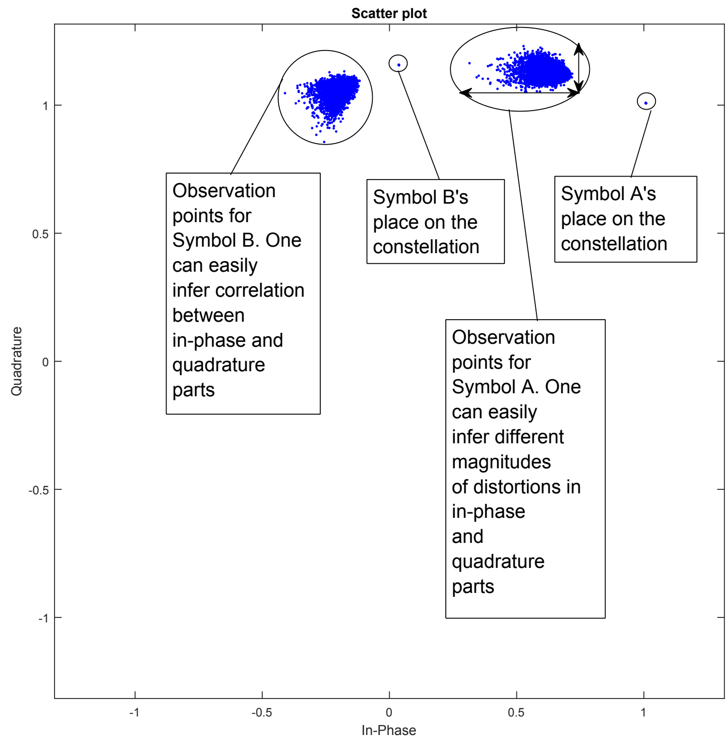

Figure 3.1: Two specific outermost constellation points' observation symbols in the receiver side

1024QAM constellation from Figure 3.2. Figure 3.2 is obtained by either utilizing a complex α or a rotation matrix.

In this thesis, a 2×2 matrix is preferred. Despite not sought here, other types of distortions such as I-Q imbalance can also be expressed with a 2×2 matrix [27]. Therefore, (3.10) can be revisited as

$$\begin{bmatrix} y^{\mathbf{I}} \\ y^{\mathbf{Q}} \end{bmatrix} = \begin{bmatrix} \alpha_{11} & \alpha_{12} \\ -\alpha_{12} & \alpha_{11} \end{bmatrix} \begin{bmatrix} x^{\mathbf{I}} \\ x^{\mathbf{Q}} \end{bmatrix} + \begin{bmatrix} w^{\mathbf{I}} \\ w^{\mathbf{Q}} \end{bmatrix}. \tag{3.13}$$

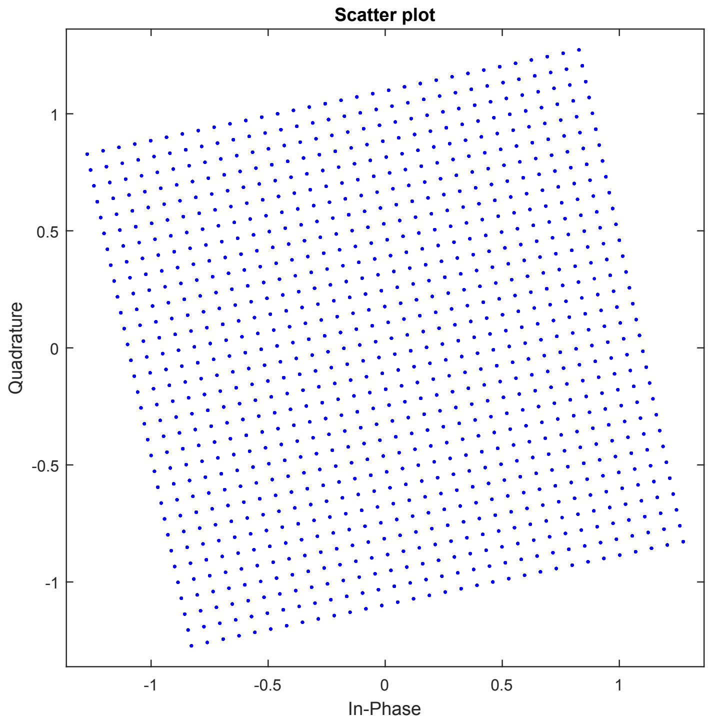

Figure 3.2: Rotation of the 1024QAM constellation with the complex α or the rotation matrix

To express all transmitted and received symbols (3.13) can be manipulated as

$$\begin{bmatrix} y_1^{\mathbf{I}} \\ y_1^{\mathbf{Q}} \\ y_2^{\mathbf{I}} \\ y_2^{\mathbf{Q}} \\ \vdots \\ y_N^{\mathbf{I}} \\ y_N^{\mathbf{Q}} \end{bmatrix} = \begin{bmatrix} x_1^{\mathbf{I}} & x_1^{\mathbf{Q}} \\ x_1^{\mathbf{Q}} & -x_1^{\mathbf{I}} \\ x_2^{\mathbf{I}} & x_2^{\mathbf{Q}} \\ x_2^{\mathbf{Q}} & -x_2^{\mathbf{I}} \\ \vdots & \vdots \\ x_N^{\mathbf{I}} & x_N^{\mathbf{Q}} \\ x_N^{\mathbf{Q}} & -x_N^{\mathbf{I}} \end{bmatrix} \begin{bmatrix} \alpha_{11} \\ \alpha_{12} \end{bmatrix} + \begin{bmatrix} w_1^{\mathbf{I}} \\ w_1^{\mathbf{Q}} \\ w_2^{\mathbf{I}} \\ w_2^{\mathbf{Q}} \\ \vdots \\ w_N^{\mathbf{I}} \\ w_N^{\mathbf{Q}} \end{bmatrix}. \tag{3.14}$$

In finding α_{11} and α_{12}, we use the least squares solution. α_{11} and α_{12} can be found as

$$\begin{bmatrix} \alpha_{11} \\ \alpha_{12} \end{bmatrix} = (\mathbf{X}^T\mathbf{X})^{-1}\mathbf{X}^T\tilde{\mathbf{y}}, \tag{3.15}$$

where $\mathbf{X} = \begin{bmatrix} x_1^{\mathbf{I}} & x_1^{\mathbf{Q}} & x_2^{\mathbf{I}} & x_2^{\mathbf{Q}} & \dots & x_N^{\mathbf{I}} & x_N^{\mathbf{Q}} \\ x_1^{\mathbf{Q}} & -x_1^{\mathbf{I}} & x_2^{\mathbf{Q}} & -x_2^{\mathbf{I}} & \dots & x_N^{\mathbf{I}} & -x_N^{\mathbf{Q}} \end{bmatrix}^T$ and

$\tilde{\mathbf{y}} = \begin{bmatrix} y_1^{\mathbf{I}} & y_1^{\mathbf{Q}} & y_2^{\mathbf{I}} & y_2^{\mathbf{Q}} & \dots & y_N^{\mathbf{I}} & y_N^{\mathbf{Q}} \end{bmatrix}^T$.

In this work our aim is to find a rotation matrix and a covariance matrix for each symbol. In other words, we obtain M rotation matrices and M covariance matrices. To do this, one cannot simply transmit a vector consisting of a_i's only with the same reasons that are explained for the Rapp model. Therefore, very long vectors of $\mathbf{x}$ and $\mathbf{y}$ are generated. Suppose there are K_i observations corresponding to symbol a_i. From (3.14), one can write the relation between a_i and its observations such that

$$\begin{bmatrix} y_{i_1}^{\mathbf{I}} \\ y_{i_1}^{\mathbf{Q}} \\ y_{i_2}^{\mathbf{I}} \\ y_{i_2}^{\mathbf{Q}} \\ \vdots \\ y_{i_{K_i}}^{\mathbf{I}} \\ y_{i_{K_i}}^{\mathbf{Q}} \end{bmatrix} = \begin{bmatrix} a_i^{\mathbf{I}} & a_i^{\mathbf{Q}} \\ a_i^{\mathbf{Q}} & -a_i^{\mathbf{I}} \\ a_i^{\mathbf{I}} & a_i^{\mathbf{Q}} \\ a_i^{\mathbf{Q}} & -a_i^{\mathbf{I}} \\ \vdots & \vdots \\ a_i^{\mathbf{I}} & a_i^{\mathbf{Q}} \\ a_i^{\mathbf{Q}} & -a_i^{\mathbf{I}} \end{bmatrix} \begin{bmatrix} \alpha_{i,11} \\ \alpha_{i,12} \end{bmatrix} + \begin{bmatrix} w_{i_1}^{\mathbf{I}} \\ w_{i_1}^{\mathbf{Q}} \\ w_{i_2}^{\mathbf{I}} \\ w_{i_2}^{\mathbf{Q}} \\ \vdots \\ w_{i_{K_i}}^{\mathbf{I}} \\ w_{i_{K_i}}^{\mathbf{Q}} \end{bmatrix} \tag{3.16}$$

where $\begin{bmatrix} y_{i_1}^{\mathbf{I}} & y_{i_1}^{\mathbf{Q}} & y_{i_2}^{\mathbf{I}} & y_{i_2}^{\mathbf{Q}} & \dots & y_{i_{K_i}}^{\mathbf{I}} & y_{i_{K_i}}^{\mathbf{Q}} \end{bmatrix}^T$ is the observation vector of a_i and $\begin{bmatrix} w_{i_1}^{\mathbf{I}} & w_{i_1}^{\mathbf{Q}} & w_{i_2}^{\mathbf{I}} & w_{i_2}^{\mathbf{Q}} & \dots & w_{i_{K_i}}^{\mathbf{I}} & w_{i_{K_i}}^{\mathbf{Q}} \end{bmatrix}^T$ is the error vector. (3.15) can be rewritten for (3.16) as

$$\begin{bmatrix} \alpha_{i,11} \\ \alpha_{i,12} \end{bmatrix} = (\mathbf{X_i}^T \mathbf{X_i})^{-1} \mathbf{X_i}^T \tilde{\mathbf{y}}_{\mathbf{i}} \tag{3.17}$$

As explained for (3.15), $\mathbf{X_i}$ and $\tilde{\mathbf{y}}_{\mathbf{i}}$ are the corresponding matrix and the corresponding vector for (3.16).

Variance of a_i's in-phase part can be calculated as

$$(\sigma_{i,\mathbf{I}}^2) = \frac{\sum_{k=1}^{K_i} |y_{i_k}^{\mathbf{I}} - \alpha_{i,11} a_i^{\mathbf{I}} - \alpha_{i,12} a_i^{\mathbf{Q}}|^2}{K_i}, \tag{3.18}$$

where $\sigma_{i,\mathbf{I}}^2$ is a measure of error magnitude of in-phase distortion , i.e., variance of in-phase error around symbol a_i. For quadrature part, $\sigma_{i,\mathbf{Q}}^2$ can be found in the same manner. Another inference from Figure 3.1 is that a correlation between in-phase and quadrature distortions may exist as observed for the constellation point B. The correlation coefficient, ρ_i, for a_i can be found as

$$\rho_i = \frac{(\mathbf{w_i^I})^T \mathbf{w_i^Q}}{K_i}. \tag{3.19}$$

where $\mathbf{w_i^I} = \begin{bmatrix} w_{i,1}^{\mathbf{I}} & w_{i,2}^{\mathbf{I}} & \dots & w_{i,N'}^{\mathbf{I}} \end{bmatrix}^T$ and $\mathbf{w_i^Q} = \begin{bmatrix} w_{i,1}^{\mathbf{Q}} & w_{i,2}^{\mathbf{Q}} & \dots & w_{i,N'}^{\mathbf{Q}} \end{bmatrix}^T$.

For M-ary QAM, the nonlinear channels can be represented with M distinct α_{x_i}, $\sigma_{x_i}^2$ and $\alpha_{i,11}$, $\alpha_{i,12}$, $\sigma_{i,\mathbf{I}}^2$, $\sigma_{i,\mathbf{Q}}^2$ and ρ_i for the Rapp and Saleh models respectively.

3.4 A Reduced Model for the Rapp model

Instead of considering each symbol's error magnitude and warping coefficient, one can also split the constellation and consider average error magnitudes or EVMs of each region. In this work, we also split the constellation as in Figure 3.3. Although, it seems that the constellation is split into 16 regions, three regions with identical characteristics appear due to symmetry. EVMs and warping coefficients of these regions can be found as they are explained in Chapter 3.2 and the receiver's performance that considers error magnitudes and warping coefficients of these regions will be presented in later parts.

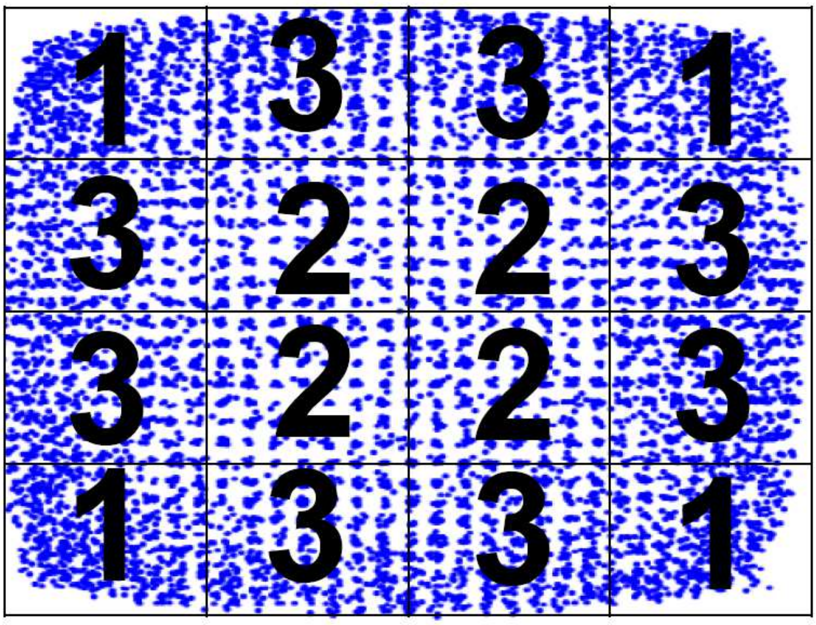

Figure 3.3: Partition of the constellation

It is worthwhile to emphasize that the constellation can also be split into more than or less than 16 regions. It may determine performance of the receiver. For this work, it is split into 16 regions.

CHAPTER 4

ACHIEVABLE RATES OF THE NONLINEAR CHANNELS

In this part, achievable rate expressions of the nonlinear channels are presented.

4.1 Mismatched Achievable Rates

For this section, the channels are defined between transmitted symbols before the pulse shaping block in Figure 2.1 and received symbols after the pulse matched filter block in Figure 2.5 with perfect sampling. The achievable rate for input symbols with uniformly distributed input is given as [28]

$$R = log_2 M - E\left[log_2\left(\frac{\sum_{x' \epsilon A_X} p(Y|x')}{p(Y|X)}\right)\right], \tag{4.1}$$

where A_X is the alphabet for the input. However, (4.1) is difficult to obtain analytically since the closed forms of $p(y)$ and $p(y|x)$ may be hard to calculate or not even exist. Therefore, the expectation in (4.1) can be calculated by Monte Carlo simulations.

Figure 4.1 depicts how one can calculate the expectation in (4.1) for the AWGN channel. This procedure is repeated many times and the mean of logarithm expressions must be taken to obtain the expectation.

Statistical distributions of the errors in (3.10) and (3.16) are not exactly Gaussian distribution. Moreover, they may not have known analytic expressions. Figure 4.2 and 4.3 show the errors' histograms which are observed around the in-phase parts of 5+5j and 27+27j for both Rapp and Saleh models. These two points are particularly chosen since 5+5j is a sample of inner constellation points and the other is one of the

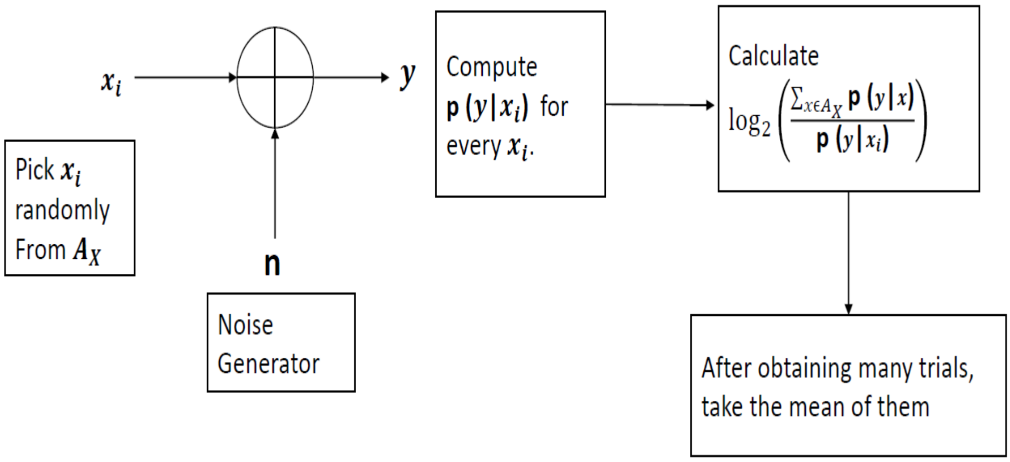

Figure 4.1: Calculation of the expectation in (4.1) for AWGN channel

outermost constellation points. From the figures, the resultant histograms do not fit with the Gaussian curves.

In the literature, some studies utilize the distribution function close to $p(y|x)$ instead of the exact $p(y|x)$. This approach is referred to as mismatched decoding and the approximate distribution function is called the mismatched PDF. Basically, a reciever decodes observations by using a mismatched likelihood function instead of an exact likelihood function. It is worthwhile to note that the receiver does not have any assumptions about statistics of observations. Observations are decoded according to the mismatched likelihood function by the receiver. In [29] and the references therein, mismatched decoding has been applied to various scenarios including ISI channels and some capacity bounds are found for this decoding as in [30]. From this point of view, the mismatched achievable rate becomes a lower bound to (4.1)

$$R_1 = log_2 M - E_{X,Y}\left[log_2\left(\frac{\sum_{x' \epsilon A_X} \widetilde{p}(Y|x')}{\widetilde{p}(Y|X)}\right)\right], \tag{4.2}$$

where $\widetilde{p}(y|x)$ is a mismatched PDF. Interesting point for (4.2) is that expectation is taken over exact statistics of X and Y, although PDF is mismatched. Expectation in (4.2) can be found by Monte Carlo simulations as found in (4.1) and Figure 4.4 illustrates procedures for finding the expectation.

For the channel model corresponding to the Rapp model, the mismatched PDF of a

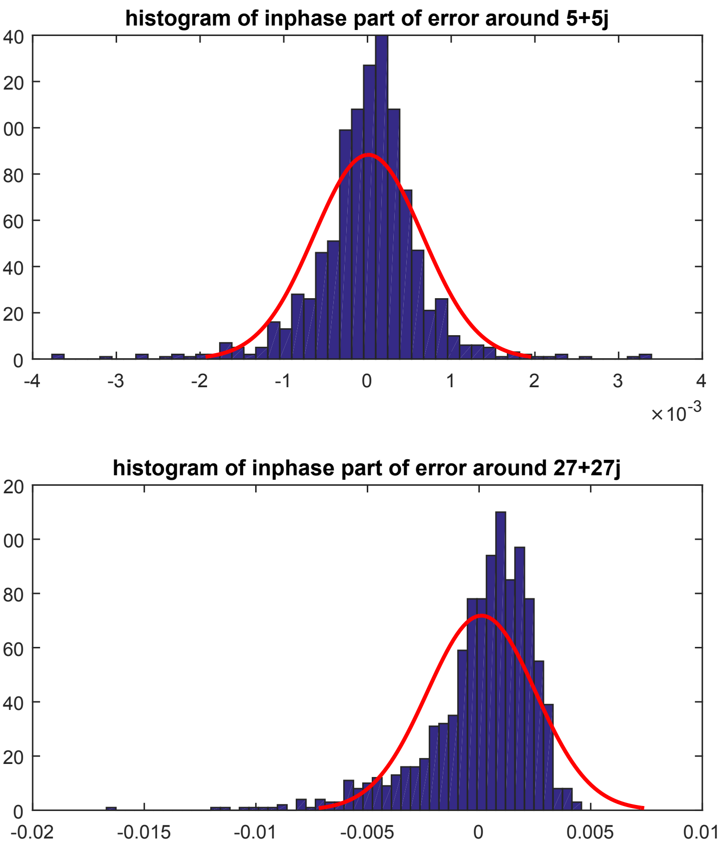

Figure 4.2: Histograms of in-phase part of error distributions around 5+5j and 27+27j for the Rapp model

particular symbol x_i can be taken as

$$\widetilde{p}(y|x_i) = \frac{1}{\pi\sigma_i^2} exp(-\frac{\|y - \alpha_{x_i} x_i\|^2}{\sigma_i^2}), \tag{4.3}$$

whereas, the mismatched PDF for the Saleh model of a particular symbol x_i can be written as

$$\widetilde{p}(\mathbf{y}|\mathbf{x_i}) = \frac{1}{\sqrt{(2\pi)^2|\mathbf{K_i}|}} exp\left(-\frac{1}{2}(\mathbf{y} - \mathbf{M_i x_i})^T \mathbf{K_i}^{-1}(\mathbf{y} - \mathbf{M_i x_i})\right), \tag{4.4}$$

where $\mathbf{y}$ and $\mathbf{x_i}$ are 2×1 vectors such that $\mathbf{y} = \begin{bmatrix} y^{\mathbf{I}} & y^{\mathbf{Q}} \end{bmatrix}^T$, $\mathbf{x_i} = \begin{bmatrix} x_i^{\mathbf{I}} & x_i^{\mathbf{Q}} \end{bmatrix}^T$, $\mathbf{M_i}$ is the 2×2 rotation matrix of symbol x_i and $\mathbf{K_i}$ is the 2×2 covariance matrix such that $\mathbf{K_i} = \begin{bmatrix} \sigma_{i,\mathbf{I}}^2 & \rho_i \\ \rho_i & \sigma_{i,\mathbf{Q}}^2 \end{bmatrix}$.

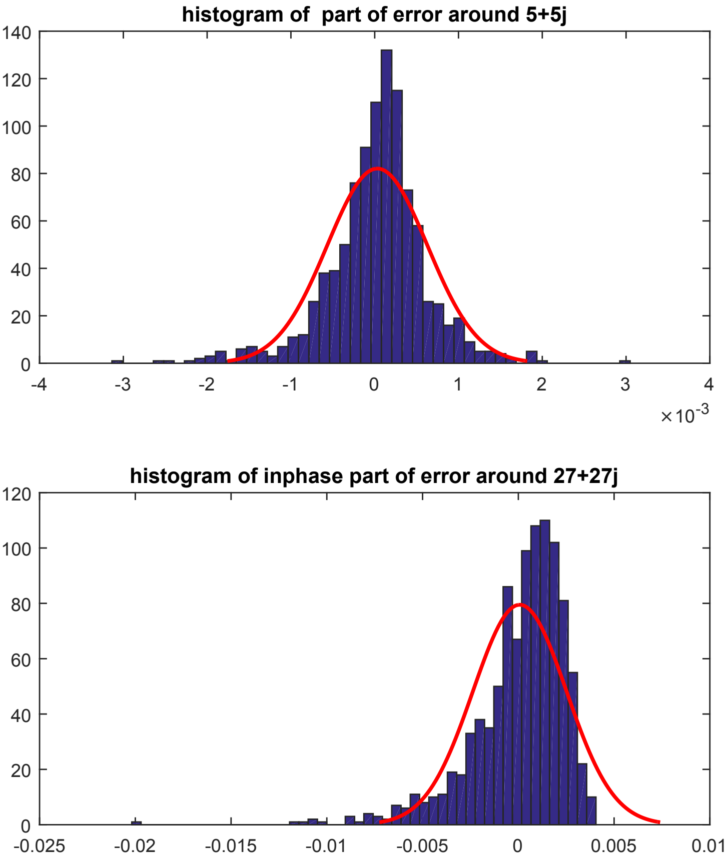

Figure 4.3: Histograms of in-phase part of error distributions around 5+5j and 27+27j for the Saleh model

4.2 Achievable Rates Based on Log Likelihood Ratios

In this part, the channels are defined between b_k, the bits after channel encoder block in Figure 2.1, and l_k, the deinterleaved LLR values after the deinterleaver block in Figure 2.5. The schematic of the channels is presented in Figure 4.5

LLR expression can be written as [31]

$$l_k = log_2 \left(\frac{P(b_k = 0|y)}{P(b_k = 1|y)} \right), \tag{4.5}$$

where b_k is k^{th} bit for an observation y. (4.5) requires too many computations in particular for high order QAM. For 4096QAM, 2048 summations are needed for both the denominator and the numerator in (4.5) for just one bit. Therefore, approximate LLR is utilized in this work without loss of generality. For the Rapp model, approximate

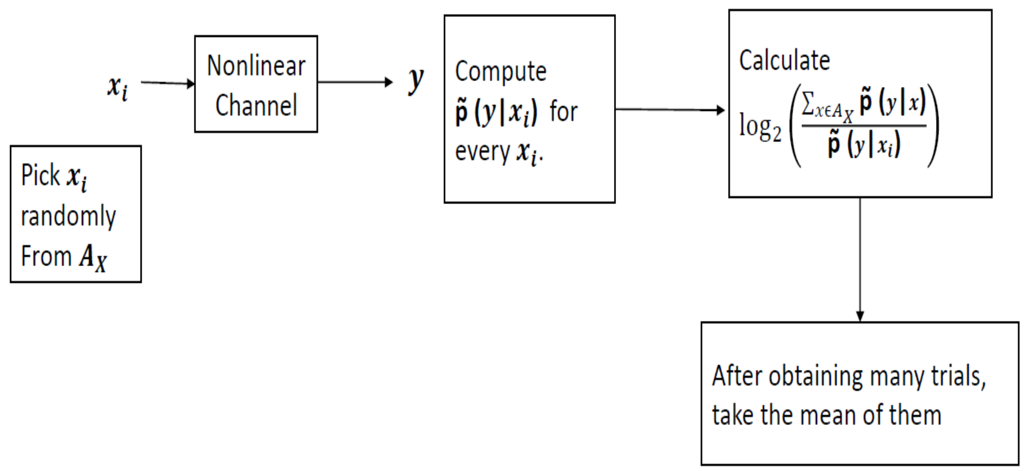

Figure 4.4: Calculation of the expectation in (4.2) for mismatched decoding

LLR can be written as

$$l_k = log_2\left(\frac{\max\limits_{x_i \epsilon X_{0,k}} \frac{1}{\pi\sigma_i^2} exp(-\frac{\|y-\alpha_{x_i}x_i\|^2}{\sigma_i^2})}{\max\limits_{x_i \epsilon X_{1,k}} \frac{1}{\pi\sigma_i^2} exp(-\frac{\|y-\alpha_{x_i}x_i\|^2}{\sigma_i^2})}\right) \tag{4.6}$$

and for the Saleh model it can be rewritten as

$$l_k = log_2\left(\frac{\max\limits_{\mathbf{x_i} \epsilon X_{0,k}} \frac{1}{\sqrt{(2\pi)^2|\mathbf{K_i}|}} exp(-\frac{1}{2}(\mathbf{y}-\mathbf{M_i x_i})^T \mathbf{K_i}^{-1}(\mathbf{y}-\mathbf{M_i x_i}))}{\max\limits_{\mathbf{x_i} \epsilon X_{1,k}} \frac{1}{\sqrt{(2\pi)^2|\mathbf{K_i}|}} exp(-\frac{1}{2}(\mathbf{y}-\mathbf{M_i x_i})^T \mathbf{K_i}^{-1}(\mathbf{y}-\mathbf{M_i x_i}))}\right), \tag{4.7}$$

where $X_{0,k}$ and $X_{1,k}$ are sets of symbols with bit 0 and 1 respectively at the given bit position k. As inferred from Chapter 2, standart gray encoded BICM scheme is utilized in this work, since BICM sturcture is practical and robust for burst errors. As stated in [32] the achievable rate of a BICM scheme can be written as

$$R_2 = \sum_{k=1}^{log_2 M} H(B_k) - H(B_k|L_k), \tag{4.8}$$

where $H(B_k)$ and $H(B_k|L_k)$ are the entropy and the conditional entropy corresponding to the kth bit. Since b_k is generated uniformly, R_2 may be written as

$$R_2 = \sum_{k=1}^{log_2 M} 1 - H(B_k|L_k). \tag{4.9}$$

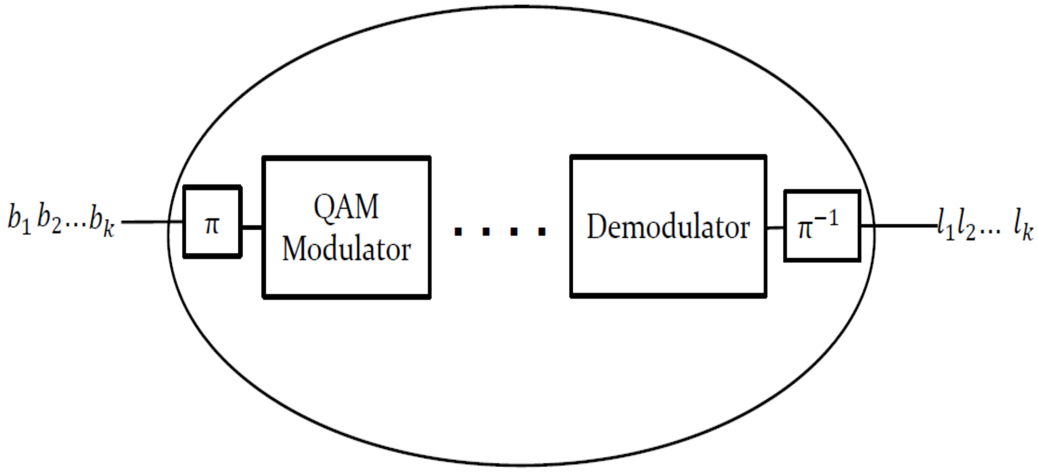

Figure 4.5: The channel schematic for Section 4.2

$H(B_k|L_k)$'s expression is

$$H(B_k|L_k) = -\int_{l_k} f(l_k) \sum_{b_k} p(b_k|l_k) log_2(p(b_k|l_k)) dl_k. \tag{4.10}$$

Since B_k is a binary random variable, one can express the summation in (4.10) with the binary entropy function

$$H_b(p) = -plog(p) - (1-p)log(1-p) \tag{4.11}$$

so that (4.10) can be rewritten as

$$H(B_k|L_k) = \int_{l_k} f(l_k) H_b(P(b_k = 0|l_k)) dl_k, \tag{4.12}$$

where $P(b_k = 0|l_k) = \frac{2^{l_k}}{1+2^{l_k}}$. In this work $H(B_k|L_k)$ is found through Monte Carlo integration since a closed form formula of $f(l_k)$ is not available.

CHAPTER 5

QUANTIZATION OF OBSERVATIONS AND SIMULATION RESULTS

In this chapter, quantization of observations are explained and then simulation results are presented.

5.1 Quantization of Observations

Obtaining LLR values for high order M-ary QAM are too complex since $M/2$ evaluations are performed to maximize the numerator and denominator of (4.6) and (4.7) for each bit. To reduce the computational complexity, we quantize the observations.

The observations are mapped to a quantization region according to the in-phase and quadrature magnitudes. There are $(m\sqrt{M})^2$ identical quantization regions where M shows modulation order and m is the resolution parameter. To illustrate, there are $(128)^2$ identical squares for 1024QAM and $m = 4$. The receivers arrange the quantization region by knowing M center of mass values of the received symbols' .Suppose that b is $\max\limits_{\substack{i=1,2,\dots,M \\ j=I,Q}} (|c_i^j|)$ where c_i^I and c_i^Q are in-phase and quadrature value of the center of mass corresponding to transmitted symbol a_i respectively. Then, each quantization region will cover a $\frac{2b}{m\sqrt{M}} \times \frac{2b}{m\sqrt{M}}$ square as depicted in Figure 5.1 that is a hypothetical figure. From Figure 5.1, all quantization regions are uniform and identical except outermost quantization regions. Outermost quantization regions extend infinity to guarantee that all observations are assigned to a quantization region. Unlike the observations as in Figure 1.1 and Figure 1.2, the quantization regions are not rotated or

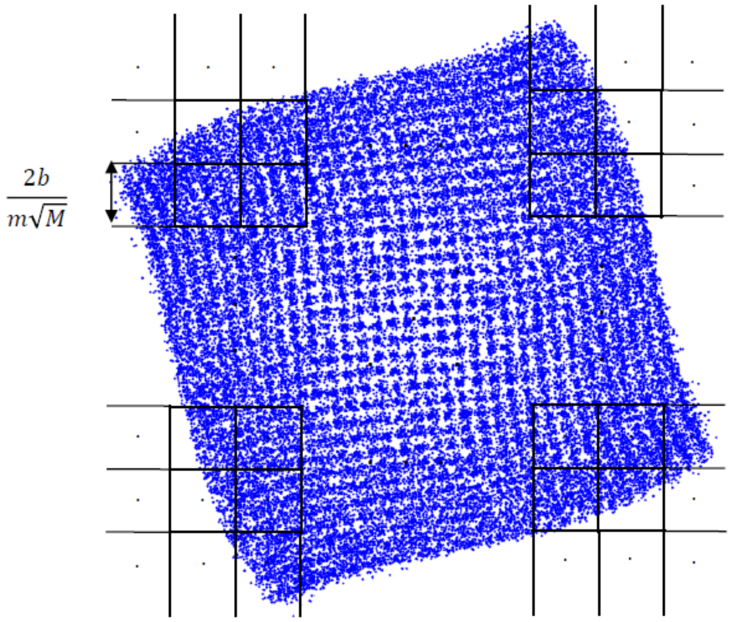

Figure 5.1: Quantization Regions

warped. Some quantization regions may be unnecessary since any observation may not be mapped to any quantization region. Optimization of the quantization regions is beyond this thesis and it can be seen as a future direction.

We desire that each quantization region has pre-computed LLR values. To do this, the points that are in the middle of each quantization region are determined. Then, the points are put into (4.6) and (4.7) for the channel of the Rapp and Saleh models respectively. (4.6) and (4.7) give LLR values of each quantization region to the receiver to form look-up table. As a result, instead of calculating (4.6) and (4.7) over and over, for each observation the quantization region is determined and the receiver reads LLR values from the look-up table.

5.2 Simulation Results

Simulation results contains performances of the receivers, achievable rates of the channels and performance of the receiver that quantizes the observations. For the simulation results, LDPC encoder produces 64800 bits in which the number of input bits for the encoder is $64800r$, r being the code rate. Each packet contains 64800 bits and 100 packets are transmitted to obtain simulation results.

5.2.1 Simulation Results For the Rapp Model

Three receiver models are compared in this part. The receiver that considers average α and σ^2 of the constellation is called the conventional receiver. The receiver that considers average α and σ^2 of three regions that is depicted in Figure 3.3 is called the 3-region receiver. The last receiver that considers α and σ^2 for each symbol is called the 1024-region receiver.

Figure 5.2 shows the six achievable rate plots as a function of the output signal power from the power amplifier. In order to determine the output back-off level, the output signal power is normalized with the maximum output power of the amplifier. From Figure 5.2, the achievable rates clearly increase when more regions are utilized by the receiver. It is also observed that achievable rates diminish with increasing the output power by incrementing the parameter G since distortion due to the nonlinearity become more effective when signal power increases. It may seem as a contradiction with [33] but Figure 5.2 does not show SNR or signal to distortion ratio. As a matter of fact, it presents the normalized output powers that restricts the rates due to the nonlinearity. For example, if one desires 8 bits/secs/Hz transmission rate for R1 of the 1024-region receiver, the normalized output power cannot exceed -3.4 dB whether the thermal noise is added or not.

In addition to these comments, as we expect from data processing inequality [34], R_1 is bigger than R_2 for all receiver types. Yet, R_1 and R_2 are very close to each other at high spectral efficiencies. When the normalized power is low, we operate in the linear region and the EVM is low. This helps obtaining high spectral efficiency and the achievable rates (R_1 and R_2) are the largest possible (10 bits/secs/Hz for 1024 QAM) and the same. On the opposite end, nonlinearity becomes effective and we start observing a difference between R1 and R2. This is the reason why R_1 and R_2 diverge at low spectral efficiency.

BER performances of the receivers with code rate 0.9 and 0.8 are plotted in Figure 5.3 with respect to the normalized output power again. -6.2 dB is the minimum output power among the six cases for error free communication. Therefore Figure 5.3 starts with -6.2 dB. When a point is missing it means that the simulations did not

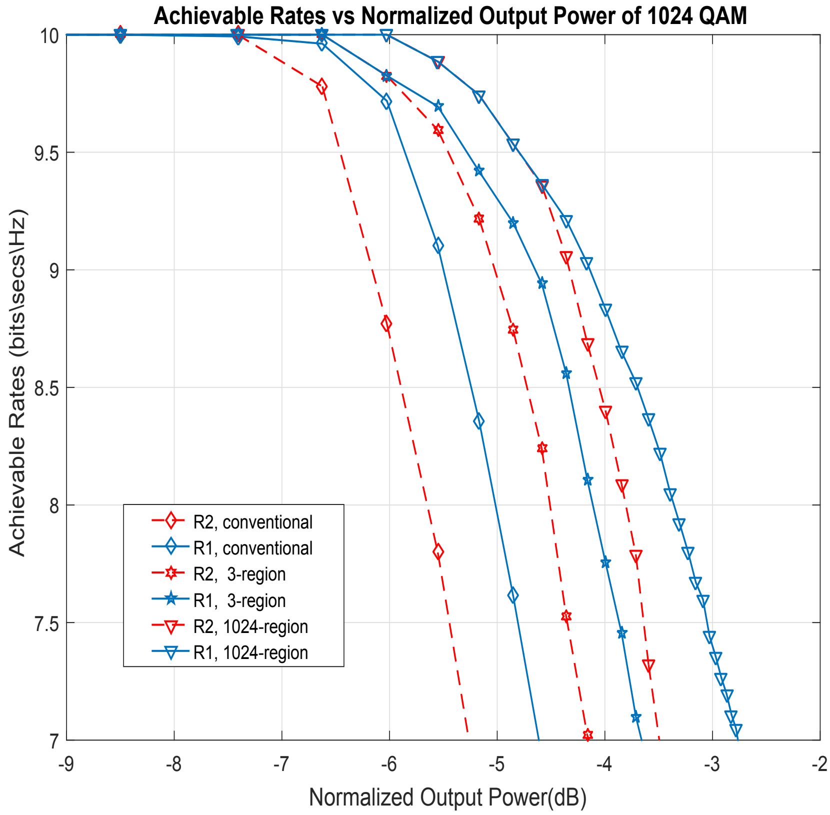

Figure 5.2: Achievable Rates of the channel for the Rapp model

produce any bit errors. From Figure 5.3 , the best performance can be obtained by the 1024-region receiver as expected. For rate 0.9, it has an advantage of roughly 0.8 dB and 1.4 dB over the 3-region receiver and the conventional receiver respectively. For rate 0.8, it will become approximately 0.6 dB and 1.4 dB gain compared with the other receivers. Although the 1024-region receiver has the best performance, its computational complexity is high since it finds and uses 1024 α and σ^2 values for the decoding. Therefore, partitioning the constellation can be seen as a compromise between complexity and performance.

One may deduce decoding thresholds from Figure 5.3 that can be compared to achievable rates. For example, the decoding threshold for code rate 0.9 with 1024 regions is -4.85 dB. We observe a 0.7 and 0.5 dB offsets in relation to R1 and R2 for the same case. Table 5.1 and 5.2 present decoding thresholds and offsets of the all receivers when the rates are 0.9 and 0.8. The observed offsets are in line with other BICM studies in the literature.

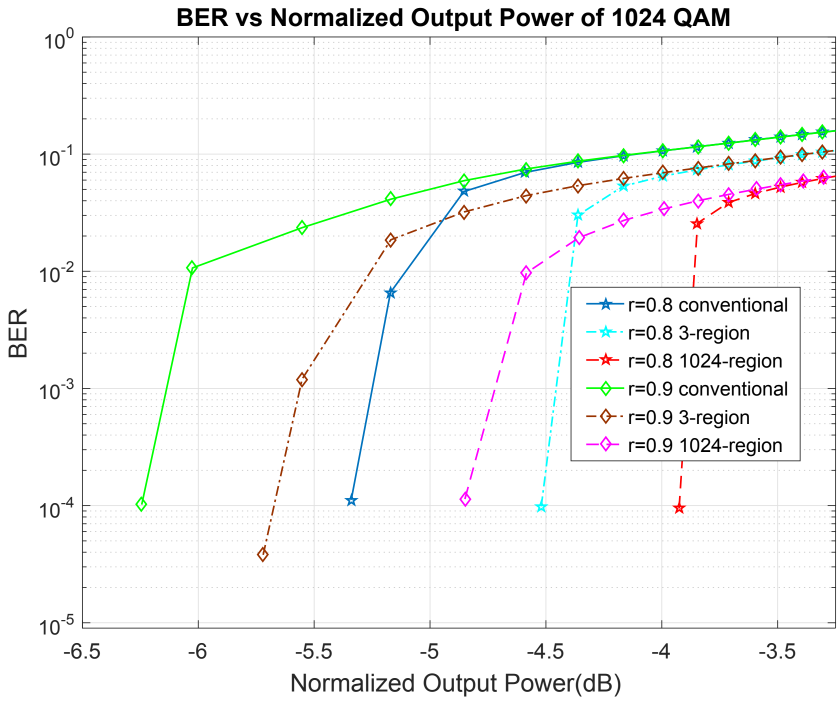

Figure 5.3: BER curves of the receivers with rate 0.8 and 0.9

Rec. Type	Output Power corresponding to 9 bits/sec/Hz of R_1 and R_2	Decoding Thr. (0.9)	Offsets
Conv.	-5.49, -6.1	-6.22	0.73, 0.12
3-region	-4.64, -5.02	-5.73	1.09, 0.71
1024-region	-4.14, -4.33	-4.86	0.72, 0.53

Table 5.1: Comparison of the reciever performances and achievable rates with $r = 0.9$

5.2.2 Simulation Results For the Saleh Model

For this part, three scenarios are considered. In the first scenario, the receiver regards the distortion as a circularly symmetric Gaussian noise term with a single rotation matrix $\mathbf{M}$ and a single variance value σ^2. The correlation between in-phase and quadrature errors is ignored. In this scenario the receiver is called the conventional receiver. In the second scenario, once again the receiver discards the correlation of the errors but rotation matrix $\mathbf{M_i}$ and variance σ_i^2 for each symbol x_i are considered by the receiver. It is also noted that the receiver distribute the variance σ_i^2 equally for both in-phase and quadrature parts. This latter receiver is called the receiver without correlation. In the last scenario, the receiver utilizes $\mathbf{M_i}$, $(\sigma_i^2)^{\mathbf{I}}$ and $(\sigma_i^2)^{\mathbf{Q}}$ for each constellation symbol and the correlation is regarded. The receiver in the last scenario

Rec. Type	Output Power corresponding to 8 bits/sec/Hz of R_1 and R_2	Decoding Thr. (0.8)	Offsets
Conv.	-5.01, -5.41	-5.43	0.42, 0.02
3-region	-4.11, -4.51	-4.52	0.41, 0.01
1024-region	-3.35, -3.81	-3.91	0.56, 0.10

Table 5.2: Comparison of the reciever performances and achievable rates with $r = 0.8$

is called the proposed receiver.

The achievable rates of the channel for the Saleh model are plotted in 5.4 with a function of normalized output power that is defined in Section 5.2.1. From Figure 5.4, the achievable rates increase when the receivers consider the correlation and the variances of in-phase and quadrature parts separately. As before, achievable rate diminishes with increasing the output power by incrementing parameter G and R_1 is greater than R_2.

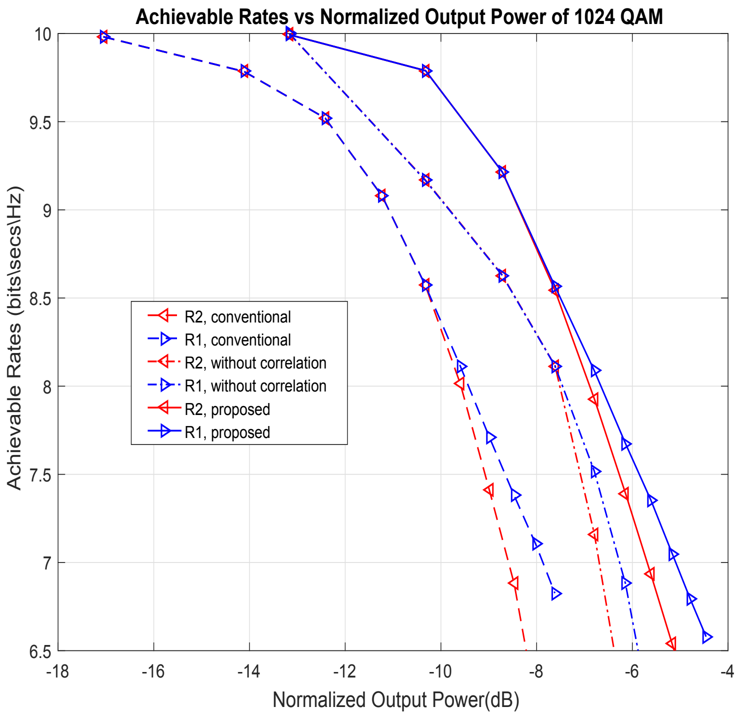

Figure 5.4: Achievable Rates of the channel for the Saleh model

Figure 5.5 shows the BER performances of the receivers with a code rate of 0.9 with respect to the normalized output power again. For error free communication the minimum output power is roughly -14.05 dB among the three receiver types. From Figure 5.5, the proposed receiver has the best performance. For rate 0.9, it has an advantage of roughly 4 dB and 2 dB over the conventional receiver and the receiver without correlation respectively at BER 10^{-3}.

Decoding thresholds can also be deduced from Figure 5.5. In order to compare receivers performances, these thresholds can be analysed with the achievable rates in Figure 5.4. To illustrate, the decoding threshold of the proposed receiver with a code rate 0.9 is -9.08 dB. There is a 0.91 dB offset in relation to achievable rate 9 bits/sec/Hz requiring -8.17 dB output power. For the receiver without correlation, the threshold and the offset become -11.94 and 2.02 dB respectively. Lastly, the threshold for the conventional receiver is -14.05 dB and 2.82 dB offset can be observed. As a result, offset increases when receiver ignores the effects such as correlation and unequal error magnitude distribution. Table 5.3 summarizes all decoding thresholds and performances of the aforementioned receivers. We observe a significant performance (5 dB) given with the proposed receiver over the conventional receiver.

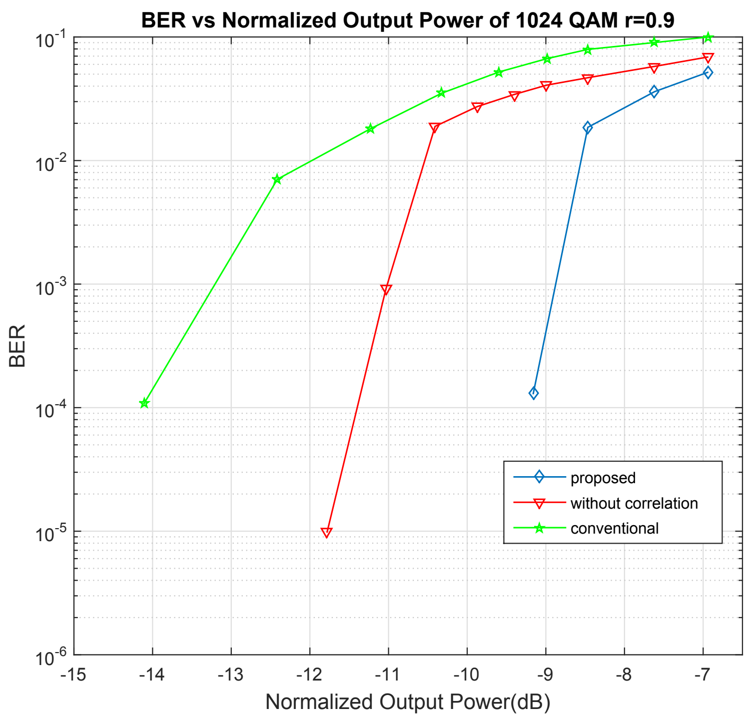

Figure 5.5: BER curves of the receivers with rate 0.9

Rec. Type	Output Power corresponding to 9 bits/sec/Hz of R_1 and R_2	Decoding Thr. (0.9)	Offsets
Conv.	-11.23	-14.05	2.82
Wto. Cor.	-9.92	-11.94	2.02
Proposed	-8.17	-9.08	0.91

Table 5.3: Comparison of the reciever performances and achievable rates with $r = 0.9$

5.2.3 Simulation Results for Receivers with Quantization

The performance of the receiver working with quantization based on look-up table is presented and compared with those of the aforementioned receivers in the previous sections. The resolution parameter, m, is taken as 2 and 4 and the code rate is taken as 0.9 for the simulations.

Figure 5.6 indicates the receivers' performances that are compared for the Rapp model. From Figure 5.6 when m increases, the performance of the 1024-region receiver with look-up table becomes closer to that of the 1024-region receiver without quantization.

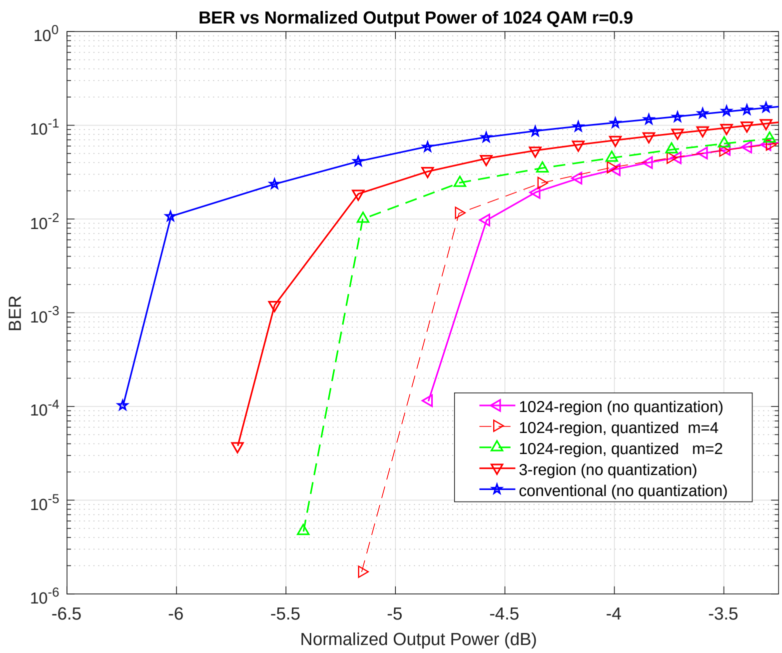

Figure 5.6: BER curves of the receivers for the Rapp model

Furthermore, when the performance of the 1024-region receiver with quantization is compared with the 3-region and the conventional receiver's performances, the 1024-region receiver with quantization may be better off even for small m. For example when $m = 2$ at BER 10^{-4}, the 1024-region receiver with quantization has 0.2 dB and 0.9 dB advantage over the unquantized 3-region and the conventional receivers respectively. When $m = 4$, this advantage becomes 0.5 dB and 1.2 dB.

Figure 5.7 shows the receivers' performances for the channel of the Saleh model. From Figure 5.7, the performance of the proposed receiver with quantization is improved by increasing m. Its performance approaches to the proposed receiver's performance without quantization when m increases. The proposed receiver with quantization has 0.8 dB and 3.1 dB over the correlation and the conventional receivers respectively, when $m = 2$ at BER 10^{-4}. For $m = 4$, this superiority becomes 2.1 dB and 4.4 dB at BER 10^{-4}.

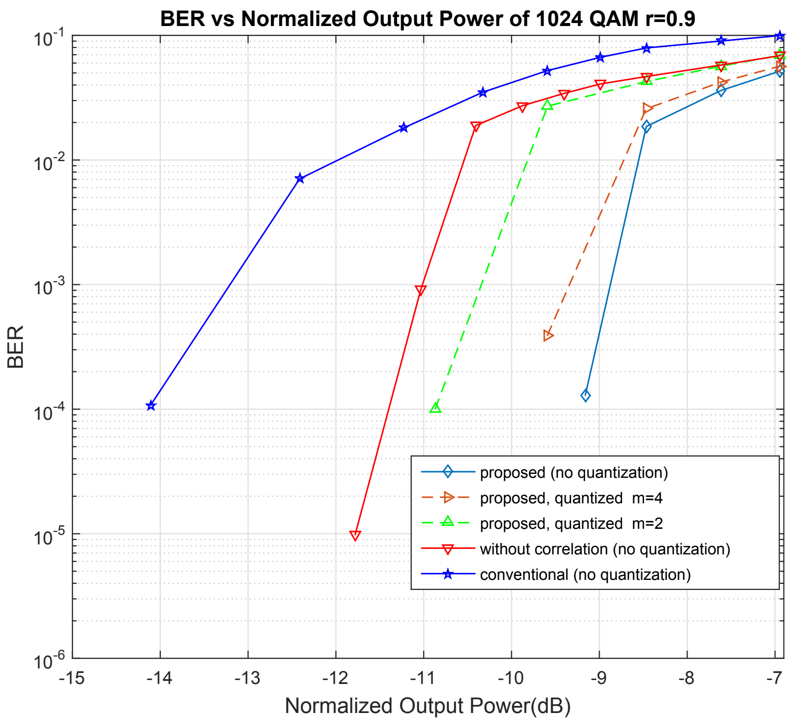

Figure 5.7: BER curves of the receivers for the Saleh model

It is worthwhile to note that the receivers with quantization set up the look-up table only once before detection operations and this reduces the computational complexity. For this work, the receivers with quantization calculate 4096 and 16384 LLR values for 1024QAM with m = 2 and m = 4, respectively. The conventional, the 3-region and without correlation receivers can also work with quantization, but this leads to performance loss and quite low performance.

CHAPTER 6

CONCLUSIONS AND FUTURE WORKS

In this thesis, effect of power amplifier nonlinearity is investigated. A power amplifier can distort transmitted signal that has high power relatively and this distortion degrades performance of a receiver. Due to this distortion, it is observed that the clouds exist around QAM symbols on the constellation and EVM of each symbol varies from symbol to symbol, that can be modelled by a variance term along with a scaling coefficient.

In this thesis, two power amplifier models that are Rapp and Saleh models are utilized to analyze and model the errors due to the nonlinearity. For the Rapp Model, the in-phase and quadrature parts of the error around particular constellation point can be assumed as independent and the error variance can be equally distributed to in-phase and quadrature parts. A practical BICM receiver that considers each symbol's error variance and power amplifier gain has the best performance among the other receivers. Instead of finding error variance for each symbol, the power amplifier gains and the error variances can be calculated for the regions by splitting the constellation as in this thesis. According to the simulation results, although complexity can be seen as the cost due to finding error variances and power amplifier gains for each symbol, the receiver that has the best performance can enhance the error rates and operate close to achievable rates.

The Saleh model is employed to examine phase distortion in conjunction with amplitude distortion. On the contrary the Rapp model, the Saleh model leads to correlation between in-phase and quadrature branches. Moreover, the Saleh model creates the errors such that variances of in-phase and quadrature parts are not equal to each other.

The simulation results show that the receiver considering the correlation and unequal in-phase/quadrature error variances outperforms other receiver schemes.

The achievable rates of the nonlinear channels are presented for both models. The achievable rates increase by considering each symbol's EVM. The receivers having the best performances can also operate close to the corresponding achievable rate values.

To avoid computational complexity in finding log-likelihood ratios, the receivers that quantize the observations based on look-up table are also proposed. Simulation results show that receivers with quantization operate with low complexity and outperform the conventional receivers.

For future works, factor graphs can be employed for detection of each symbol by considering each symbol's ISI channel separately and the resultant performance can be compared with nonlinear Volterra equalizers. Moreover, the detection schemes that are proposed in this work can be adapted for massive multiple input multiple output systems with different scenarios.

REFERENCES

[1] C. Dehos, J. L. González, A. D. Domenico, D. Kténas, and L. Dussopt, "Millimeter-wave access and backhauling: the solution to the exponential data traffic increase in 5g mobile communications systems," *IEEE Commun. Mag.*, vol. 52, pp. 88–95, Sep. 2014.

[2] W. Hong, K. H. Baek, Y. Lee, Y. Kim, and S. T. Ko, "Study and prototyping of practically large-scale mmwave antenna systems for 5g cellular devices," *IEEE Commun. Mag.*, vol. 52, pp. 63–69, Sep. 2014.

[3] C. E. Burnet and W. G. Cowley, "Performance analysis of turbo equalization for nonlinear channels," in *Proc. IEEE Int. Symp. on Information Theory*, pp. 2026–2030, Sep. 2005.

[4] D. R. Morgan, Z. Ma, J. Kim, M. G. Zierdt, and J. Pastalan, "A generalized memory polynomial model for digital predistortion of rf power amplifiers," *IEEE Trans. Signal Process.*, vol. 54, pp. 3852–3860, Oct. 2006.

[5] C. F. Cheang, K. F. Un, W. H. Yu, P. I. Mak, and R. P. Martins, "A combinatorial impairment-compensation digital predistorter for a sub-ghz ieee 802.11af-wlan cmos transmitter covering a 10x-wide rf bandwidth," *IEEE Trans. Circuits Syst. I: Reg. Papers*, vol. 62, pp. 1025–1032, Apr. 2015.

[6] Y. Liu, G. Liu, and P. M. Asbeck, "High-order modulation transmission through frequency quadrupler using digital predistortion," *IEEE Trans. Microw. Theory Techn.*, vol. 64, pp. 1896–1910, Jun. 2016.

[7] H. T. Dabag, B. Hanafi, O. D. Gürbüz, G. M. Rebeiz, J. F. Buckwalter, and P. M. Asbeck, "Transmission of signals with complex constellations using millimeter-wave spatially power-combined cmos power amplifiers and digital predistortion," *IEEE Trans. Microw. Theory Techn.*, vol. 63, pp. 2364–2374, Jul. 2015.

[8] D. J. C. MacKay and R. M. Neal, "Near shannon limit performance of low density parity check codes," *Electron. Lett.*, vol. 32, pp. 1645–, Aug. 1996.

[9] A. Martinez, A. G. i Fabregas, G. Caire, and F. M. J. Willems, "Bit-interleaved coded modulation in the wideband regime," *IEEE Trans. Inf. Theory*, vol. 54, pp. 5447–5455, Dec. 2008.

[10] C. Rapp, "Effects of HPA-nonlinearity on a 4-DPSK/OFDM-signal for a digital sound broadcasting signal," in *Rec. Conf. ECSC'91 Liege*, pp. 179–184, 1991.

[11] E. Köken and A. Ö. Yılmaz, "Spectral mask compliance and amplifier nonlinearity in single carrier and ofdm systems," *Wireless Personal Communications*, vol. 63, pp. 579–586, Apr 2012.

[12] A. A. M. Saleh, "Frequency-independent and frequency-dependent nonlinear models of TWT amplifiers," *IEEE Trans. Commun.*, vol. 29, pp. 1715–1720, Nov. 1981.

[13] E. Costa, M. Midrio, and S. Pupolin, "Impact of amplifier nonlinearities on ofdm transmission system performance," *IEEE Commun. Lett.*, vol. 3, pp. 37–39, February 1999.

[14] C.-P. Liang, J.-H. Jong, W. E. Stark, and J. R. East, "Nonlinear amplifier effects in communications systems," *IEEE Trans. Microw. Theory Techn.*, vol. 47, pp. 1461–1466, Aug. 1999.

[15] L. G. Baltar, D. S. Waldhauser, and J. A. Nossek, "Out-of-band radiation in multicarrier systems: A comparison," in *Multi-Carrier Spread Spectrum 2007* (S. Plass, A. Dammann, S. Kaiser, and K. Fazel, eds.), (Dordrecht), pp. 107–116, Springer Netherlands, 2007.

[16] S. Dimitrov, "Non-linear distortion noise cancellation for satellite return links," in *Proc. IEEE Int. Conf. Commun. (ICC)*, pp. 1–6, May 2016.

[17] J. Proakis and M. Salehi, *Digital Communications*. McGraw-Hill, 2008.

[18] V. Volterra, *Theory of Functionals and of Integral and Integro-differential Equations*. Dover Books on Mathematics Series, Dover Publications, 2005.

[19] A. Gutierrez and W. E. Ryan, "Performance of adaptive Volterra equalizers on nonlinear satellite channels," in *Proc. IEEE Int. Conf.Commun.*, vol. 1, pp. 488–492 vol.1, Jun. 1995.

[20] S. Benedetto and E. Biglieri, "Nonlinear equalization of digital satellite channels," *IEEE J. Sel. Areas Commun.*, vol. 1, pp. 57–62, Jan. 1983.

[21] G. Colavolpe and A. Piemontese, "Novel SISO detection algorithms for nonlinear satellite channels," *IEEE Wireless Commun. Lett.*, vol. 1, pp. 22–25, Feb. 2012.

[22] T. Marzetta, E. Larsson, H. Yang, and H. Ngo, *Fundamentals of Massive MIMO*. Cambridge University Press, 2016.

[23] E. Biglieri, R. Calderbank, A. Constantinides, A. Goldsmith, A. Paulraj, and H. Poor, *MIMO Wireless Communications*. Cambridge University Press, 2007.

[24] A. Goldsmith, *Wireless Communications*. Cambridge University Press, 2005.

[25] V. A. Thomas, S. Kumar, S. Kalyani, M. El-Hajjar, K. Giridhar, and L. Hanzo, "Error vector magnitude analysis of fading SIMO channels relying on MRC reception," *IEEE Trans. on Commun.*, vol. 64, pp. 1786–1797, Apr. 2016.

[26] R. Vandebril, M. Van Barel, and N. Mastronardi, *Matrix Computations and Semiseparable Matrices: Eigenvalue and Singular Value Methods*. Johns Hopkins University Press, 2010.

[27] M. Valkama, M. Renfors, and V. Koivunen, "Advanced methods for I/Q imbalance compensation in communication receivers," *IEEE Trans. Signal Process.*, vol. 49, pp. 2335–2344, Oct 2001.

[28] G. Ungerboeck, "Channel coding with multilevel/phase signals," *IEEE Trans. Inf. Theory*, vol. 28, pp. 55–67, Jan. 1982.

[29] A. Modenini, F. Rusek, and G. Colavolpe, "Optimal transmit filters for ISI channels under channel shortening detection," *IEEE Trans. Commun.*, vol. 61, pp. 4997–5005, Dec. 2013.

[30] A. Lapidoth, "Mismatched decoding and the multiple-access channel," *IEEE Trans. Inf. Theory*, vol. 42, pp. 1439–1452, Sep. 1996.

[31] S. Allpress, C. Luschi, and S. Felix, "Exact and approximated expressions of the log-likelihood ratio for 16-QAM signals," in *Proc. 38th Asilomar Conf. Signal, Syst. Comput*, vol. 1, pp. 794–798 Vol.1, Nov. 2004.

[32] G. Caire, G. Taricco, and E. Biglieri, "Bit-interleaved coded modulation," *IEEE Trans. Inf. Theory*, vol. 44, pp. 927–946, May 1998.

[33] C. E. Shannon, "A mathematical theory of communication," *The Bell System Technical Journal*, vol. 27, pp. 379–423, Jul. 1948.

[34] T. M. Cover and J. A. Thomas, *Elements of Information Theory (Wiley Series in Telecommunications and Signal Processing)*. New York, NY, USA: Wiley-Interscience, 2006.